JACS
JOURNAL OF THE AMERICAN CHEMICAL SOCIETY

Article

pubs.acs.org/JACS

Isotropic and Anisotropic Growth of Metal–Organic Framework (MOF) on MOF: Logical Inference on MOF Structure Based on Growth Behavior and Morphological Feature

Sora Choi, Taeho Kim, Hoyeon Ji, Hee Jung Lee, and Moonhyun Oh*

Department of Chemistry, Yonsei University, 50 Yonsei-ro, Seodaemun-gu, Seoul 120-749, Korea

Supporting Information

ABSTRACT: The growth of one metal–organic framework (MOF) on another MOF for constructing a heterocompositional hybrid MOF is an interesting research topic because of the curiosity regarding the occurrence of this phenomenon and the value of hybrid MOFs as multifunctional materials or routes for fine-tuning MOF properties. In particular, the anisotropic growth of MOF on MOF is fascinating for the development of MOFs possessing atypical shapes and heterostructures or abnormal properties. Herein, we clarify the understanding of growth behavior of a secondary MOF on an initial MOF template, such as isotropic or anisotropic ways associated with their cell parameters. The isotropic growth of MIL-68-Br on the MIL-68 template results in the formation of core–shell-type MIL-68@MIL-68-Br. However, the unique anisotropic growth of a secondary MOF (MOF-NDC) on the MIL-68 template results in semitubular particles, and structural features of this unknown secondary MOF are successfully speculated for the first time on the basis of its unique growth behavior and morphological characteristics. Finally, the validation of this structural speculation is verified by the powder X-ray diffraction and the selected area electron diffraction studies. The results suggests that the growth behavior and morphological features of MOFs should be considered to be important factors for understanding the MOFs' structures.

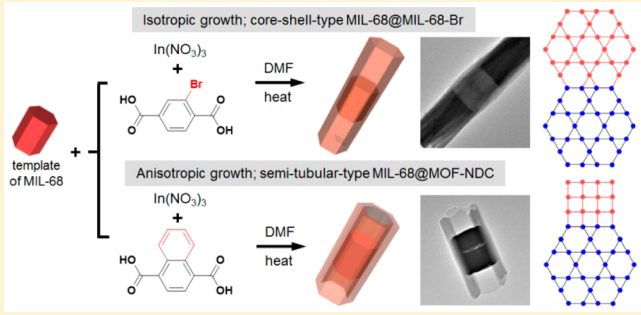

INTRODUCTION

Metal–organic frameworks (MOFs) and porous coordination polymers (CPs) have received great attention not only because of their various structural topologies and chemical tunabilities but also because of their several useful properties and applications, such as gas storage, gas separation, catalysis, sensing, and recognition.[1−12] The researchers are attempting to produce micro- or nanoscaled CP particles (CPPs)[13−22] including micro- or nano-MOFs because these materials can extend application areas or enhance the properties of the original CPs and MOFs. Indeed, micro- or nanoscaled CPPs and MOFs display enhanced properties and have been utilized in unique application areas such as magnetic resonance imaging (MRI) contrast agents, drug delivery vessels, and biosensing.[18−22]

The conjugation of MOF materials with other materials, such as silica, polystyrene, magnetic particles, and noble metal particles,[23−28] is a noble strategy for producing MOF-based functional materials. Not only the conjugation of MOFs with other materials but also the controlled conjugation of MOFs with different types of MOFs[29−34] to form hybrid MOFs containing more than two types of MOFs in one particle is a central goal in MOF development; this is because the management of the composition and structure of MOFs is essential to fine-tuning their properties. These hybrid MOF materials with precise heterocompositions or heterostructures will provide great opportunities to overcome their inherent weak points or to obtain a user's desirable properties. However, not many studies have examined the construction of hybrid MOFs through the continuous growth of a secondary MOF on an initial MOF.[30−34] In particular, there are only a few examples for understanding hybrid MOF formation through the anisotropic growth of MOF on MOF,[33,34] and the creation of a well-defined heterointerface between two completely different MOFs has rarely been demonstrated. Herein, we report the investigation of the isotropic and anisotropic growth of two MOFs, named MIL-68-Br (MIL stands for Materials of Institut Lavoisier) and MOF-NDC (NDC stands for naphthalene-1,4-dicarboxylic acid), on a microsized MOF template made from MIL-68. The isotropic growth of MIL-68-Br on the MIL-68 template resulted in core–shell-type MIL-68@MIL-68-Br. In addition, the fascinating anisotropic growth of MOF-NDC on the MIL-68 template resulted in the formation of unusual semitubular particles. In particular, the crystal structure of a new MOF (MOF-NDC) was speculated on the basis of its unique growth behavior and morphological features, and the speculated structure was validated from powder X-ray diffraction (PXRD) and selected-area electron diffraction (SAED) studies.

Received: August 23, 2016
Published: October 11, 2016

DOI: 10.1021/jacs.6b08821
J. Am. Chem. Soc. 2016, 138, 14434−14440

Scheme 1. Solvothermal Reactions for the Synthesis of CPP-I-CPP-III[a]

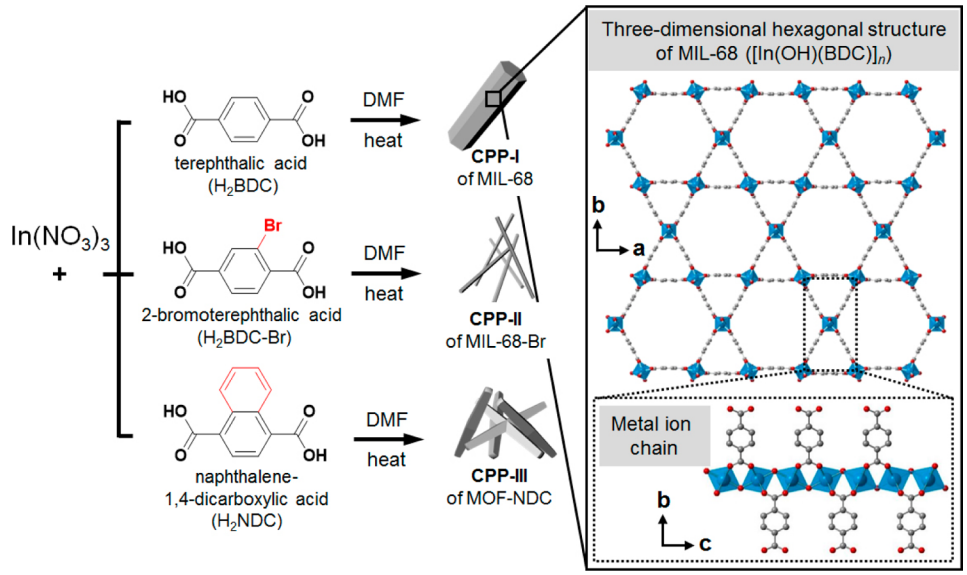

[a]The box shows ball-and-stick representations of the MIL-68 structure, which has a three-dimensional hexagonal structure of $[In(OH)(BDC)]_n$, consisting of a one-dimensional metal ion chain in the *c* direction.

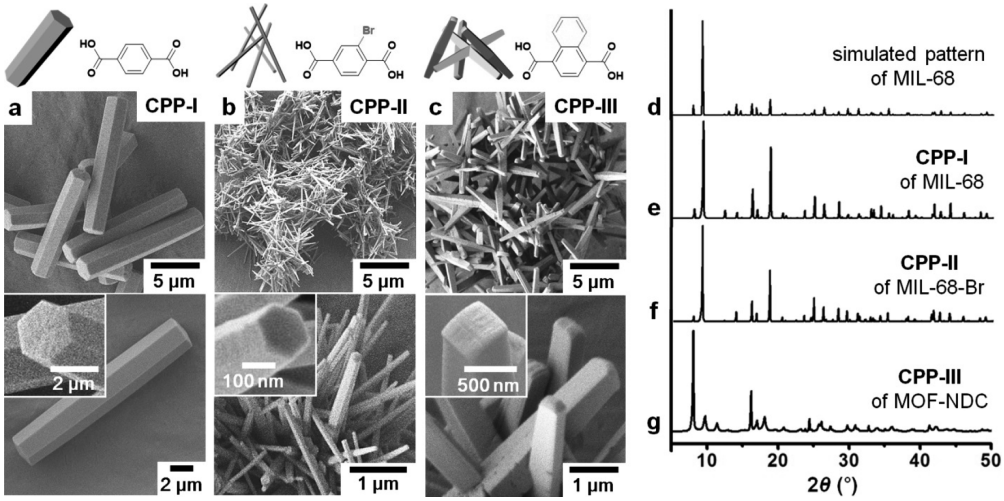

Figure 1. SEM images of (a) hexagonal rods of **CPP-I**, (b) thin hexagonal rods of **CPP-II**, and (c) rectangular rods of **CPP-III**. The insets in a and b show the hexagonal facets, and the inset in c shows a square facet. (d) Simulated PXRD pattern of MIL-68 and PXRD patterns of (e) **CPP-I**, (f) **CPP-II**, and (g) **CPP-III**.

RESULTS AND DISCUSSION

Three CPPs were first constructed from the solvothermal reactions of $In(NO_3)_3$ with one of the following three different but similar organic building blocks: terephthalic acid (benzene dicarboxylic acid, H_2BDC), 2-bromoterephthalic acid (H_2BDC-Br), and naphthalene-1,4-dicarboxylic acid (H_2NDC) (Scheme 1). Technically, the three organic building blocks have identical lengths from one side of the carboxylic acid group to the other (Scheme 1); therefore, structural and/or morphological similarities among the three CPPs made from these organic building blocks can be expected. The three CPPs were first characterized by scanning electron microscopy (SEM) and PXRD (Figure 1). First, it should be noted that the hexagonal rods of MIL-68 (**CPP-I**, Figure 1a), which has a three-dimensional hexagonal structure of $[In(OH)(BDC)]_n$ consisting of a one-dimensional metal ion chain in the *c* direction (box in Scheme 1), resulted from the solvothermal reaction of $In(NO_3)_3$ and H_2BDC.[35,36] A similar reaction of H_2BDC-Br instead of H_2BDC with $In(NO_3)_3$ resulted in the formation of thin microrods (**CPP-II**, Figure 1b). Even the resulting **CPP-II** is quite thin; it also has hexagonal facets (bottom of Figure 1b) characteristic of the MIL-68 structure. In addition, **CPP-II** displayed a PXRD pattern (Figure 1f) almost identical to that of **CPP-I** (Figure 1e) and a simulated PXRD pattern of MIL-68 (Figure 1d). These data clearly support the fact that **CPP-II** has a three-dimensional hexagonal structure (denoted as MIL-68-Br), similar to the MIL-68 structure of **CPP-I**. Overall, this indicates that the bromo moieties within H_2BDC-Br building blocks did not affect the structural or morphological change in CPPs synthesized from H_2BDC-Br.

On the other hand, the solvothermal reaction of $In(NO_3)_3$ and H_2NDC resulted in the formation of thin rods (**CPP-III**, Figure 1c). Importantly, these rods have square facets instead of the characteristic hexagonal facets of the MIL-68 structure. The

DOI: 10.1021/jacs.6b08821
J. Am. Chem. Soc. 2016, 138, 14434−14440

morphological features of **CPP-III** will aid in understanding its structural features as well as its growth behavior on the MIL-68 template. Unlike **CPP-I** and **CPP-II** of the three-dimensional hexagonal MIL-68 structures, **CPP-III** has a quite distinguishable PXRD pattern (Figure 1g); therefore, we can imagine that its structure (denoted as MOF-NDC) is different from the MIL-68 structure. The additional bulky aromatic rings of the NDC building blocks compared to the BDC building blocks may interrupt the formation of the MIL-68-like structure. The exact crystal structure of a new MOF-NDC was not available at this point because the preparation of a good single crystal was not successful. However, the speculation of structural features of MOF-NDC on the basis of its unique growth behavior and morphological features, and the analysis of its PXRD and SAED patterns will be discussed later (Figures 4, 5, and 7).

The gas sorption properties of the resulting three CPPs were obtained from their N_2 sorption isotherms. **CPP-I** of the MIL-68 structure is known to be a quite porous material,[36] as shown in its sorption isotherms [red line in Figure S1; the Brunauer–Emmett–Teller (BET) surface area and total pore volume were 1564 $m^2\ g^{-1}$ and 0.69 $cm^3\ g^{-1}$, respectively]. The BET surface area and total pore volume of **CPP-II** of the MIL-68-Br structure (1062 $m^2\ g^{-1}$ and 0.47 $cm^3\ g^{-1}$, respectively) were slightly lower than those of **CPP-I** because of the bromo moieties within the MIL-68-Br structure (blue line in Figure S1 and Table S1). Compared to **CPP-I** made from H_2BDC, the extra bromo moieties within **CPP-II** decrease the void volume within the structure and increase the relative weight per unit volume, thereby reducing the total pore volume per gram of **CPP-II**. N_2 sorption isotherms of **CPP-III** of the MOF-NDC structure also displayed type I behavior, typical of microporous materials (purple line in Figure S1), and its BET surface area and total pore volume (597 $m^2\ g^{-1}$ and 0.27 $cm^3\ g^{-1}$, respectively) were lower than those of **CPP-I** and **CPP-II** (Table S1). Pore size distributions of **CPP-I**–**CPP-III** were calculated from the nonlocal density functional theory (NLDFT) method (Figure S2). **CPP-I** and **CPP-II** have two different pores (ca. 0.6 and 1.2 nm); however, **CPP-III** has only one dominant pore at ca. 0.7 nm. Thermogravimetric analysis (TGA) curves and infrared (IR) spectra of all samples are shown in Figures S3 and S4. Three CPPs (**CPP-I**–**CPP-III**) have a similar thermal stability, as shown in their TGA curves (Figure S3).

As an essential subject, we have investigated the growth behaviors of MOFs on the surface of a micro-MOF template (Scheme 2). The micro-MOF template of MIL-68 (Figure 2a and Figure S5a) as a short version of **CPP-I** was first prepared using a previously reported synthesis method.[36] The isotropic growth of MIL-68-Br on the MIL-68 template to produce core–shell-type MIL-68@MIL-68-Br is foreseeable because the initial MIL-68 template and the secondary MIL-68-Br have virtually identical structures, as verified from their PXRD patterns (Figure S5a and Figure 1f); therefore, the MOF system cannot recognize the fact that the organic building block was changed from BDC to BDC-Br. Indeed, the PXRD pattern (Figure S5b) of the core–shell-type **hybrid-CPP-II** of MIL-68@MIL-68-Br displayed exactly the same PXRD pattern as the initial MIL-68 template (Figure S5a). SEM images (Figure 2) revealed the formation of long hexagonal rods (**hybrid-CPP-II**) as a result of the isotropic growth of the secondary MIL-68-Br on the MIL-68 template. With increasing time, the length of the product dramatically increased, with a small increase in thickness compared to that of the initial hexagonal lump template (Figure 2d). There was no pure MIL-68 template remaining after the reaction, and there was no significant pure

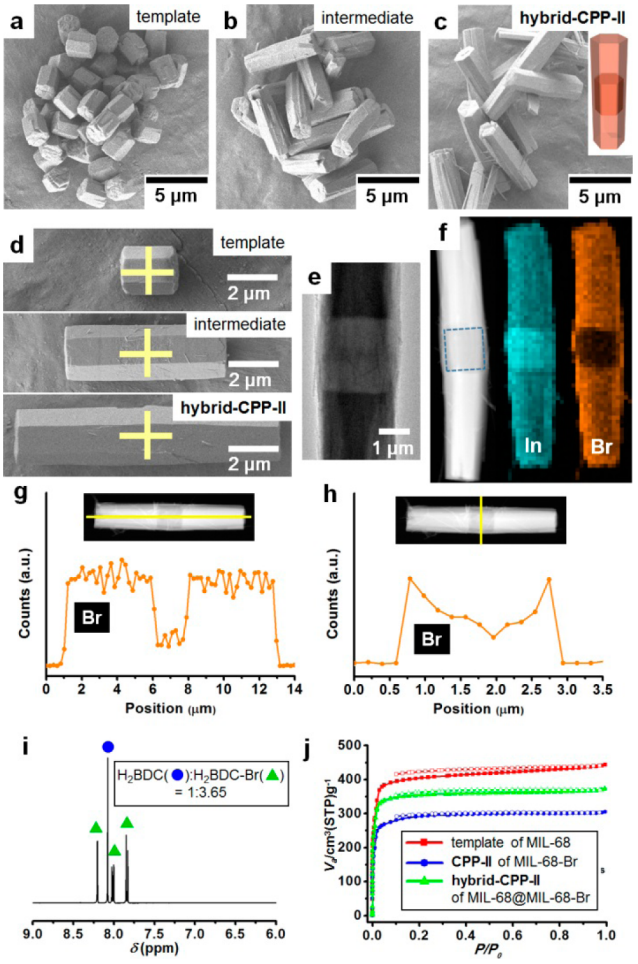

Figure 2. SEM images of (a) the initial microtemplates of MIL-68, (b) the intermediates, and (c) the core–shell-type **hybrid-CPP-II** of MIL-68@MIL-68-Br. (d) SEM images showing the particle growth. (e) TEM image and (f) STEM image, with the elemental mapping images of In (green) and Br (orange) of **hybrid-CPP-II**. (g, h) EDX spectrum profile scanning data for the bromine atom of **hybrid-CPP-II** of MIL-68@MIL-68-Br. (i) ^1H NMR spectrum of **hybrid-CPP-II** digested in acetic acid-d_4 and DMSO-d_6. (j) Comparison of N_2 sorption isotherms of the template (MIL-68, red), **CPP-II** (MIL-68-Br, blue), and **hybrid-CPP-II** (MIL-68@MIL-68-Br, green).

Scheme 2. Schematic Representation for Constructing Core–Shell-Type and Semitubular-Type Hybrid-CPPs through Isotropic and Anisotropic Growth of the Secondary MOFs on the MIL-68 Template, Respectively

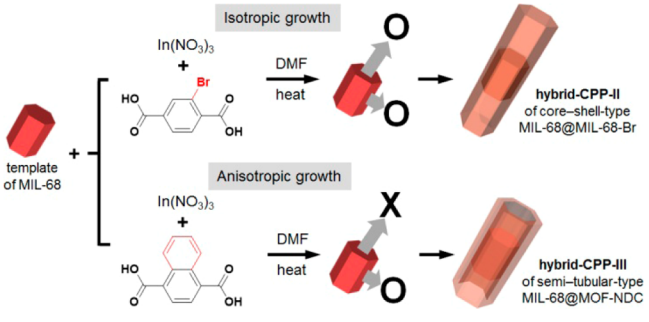

DOI: 10.1021/jacs.6b08821
J. Am. Chem. Soc. 2016, 138, 14434–14440

MIL-68-Br generated after the reaction. The contrast light and shade transmission electron microscopy (TEM) and scanning TEM (STEM) images (Figure 2e,f) of **hybrid-CPP-II** well depicted an MIL-68 template core portion and a newly grown MIL-68-Br shell portion, indicating the formation of core–shell-type MIL-68@MIL-68-Br. Noticeably, the elemental mapping images (Figure 2f) showed a core–shell structure where bromine atoms exist in the entire particle, with weak distribution in the center of the particle. In addition, EDX spectrum profile scanning data of **hybrid-CPP-II** (Figure 2g,h) confirmed the formation of well-structured core–shell-type MIL-68@MIL-68-Br. Bromine atoms, as a component of the MIL-68-Br shell, were distributed over the entire particle; however, they were dominant at the edge of the rod, which is a typical distribution tendency for the shell portion within a core–shell structure (Figure 2g,h).

The relative amounts of the MIL-68 core and MIL-68-Br shell within MIL-68@MIL-68-Br were determined from the ^{1}H NMR spectrum. First, **hybrid-CPP-II** was digested in a cosolvent of acetic acid-d_4 and DMSO-d_6; the relative ratio of H_2BDC to H_2BDC-Br and thus the relative amounts of the MIL-68 core and MIL-68-Br shell within **hybrid-CPP-II** were determined to be 1:3.65 by integrating the peaks correlated to H_2BDC and H_2BDC-Br (Figure 2i). N_2 sorption isotherms of **hybrid-CPP-II** (green line in Figure 2j) revealed that its BET surface area (1346 m^2g^{-1}) and total pore volume (0.58 $cm^3\ g^{-1}$, Table S1) values are situated roughly between those of MIL-68 (red line in Figure 2j) and MIL-68-Br (blue line in Figure 2j).

The next attempt to investigate the growth of MOF on MOF was conducted using H_2NDC as an organic building block. First, it should be mentioned that a totally different framework (MOF-NDC) was constructed from the reaction of $In(NO_3)_3$ and H_2NDC, compared to the formation of MIL-68-like structures from H_2BDC and H_2BDC-Br. SEM images (Figure 3) of **hybrid-CPP-III** revealed an obvious increase in particle size and the exclusive formation of the fascinating semitubular particles after 20 min. The pure MIL-68 template did not remain after the reaction, and the significant pure MOF-NDC was not generated after the reaction. The formation of the semitubular particles was clearly confirmed again from TEM images (Figure 3d). These semitubular particles can be constructed from the anisotropic growth of the secondary MOF-NDC on the six rectangular facets but not on the two hexagonal facets of hexagonal lump templates of MIL-68. After the initial formation of MOF-NDC on the *ac* plane of the template, MOF-NDC can further grow along the *c* axis to form semitubular particles. As the reaction time or the amounts of H_2NDC and $In(NO_3)_3$ increased, the resulting particle size of **hybrid-CPP-III** increased while retaining the semitubular shape (Figure S6). As a control experiment, the growth of MIL-68 on the MOF-NDC template resulted in similar semitubular particles (Figure S7). The PXRD pattern of **hybrid-CPP-III** (Figure 4b) showed the coexistence of both MIL-68 and MOF-

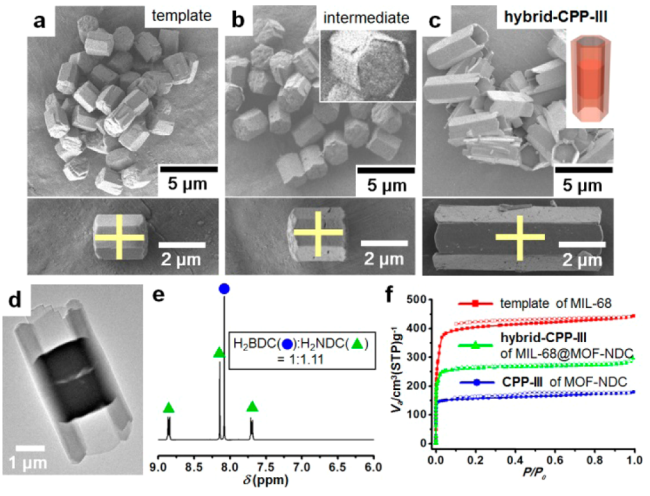

Figure 3. SEM images of (a) the initial microtemplates of MIL-68 and (b) the intermediates. (c) SEM and (d) TEM images of **hybrid-CPP-III** of semitubular-type MIL-68@MOF-NDC. The bottom images in a–c clearly show the particle growth. (e) ^{1}H NMR spectrum of **hybrid-CPP-III** digested in acetic acid-d_4 and DMSO-d_6. (f) Comparison of N_2 sorption isotherms of the template (MIL-68, red), **CPP-III** (MOF-NDC, blue), and **hybrid-CPP-III** (MIL-68@MOF-NDC, green).

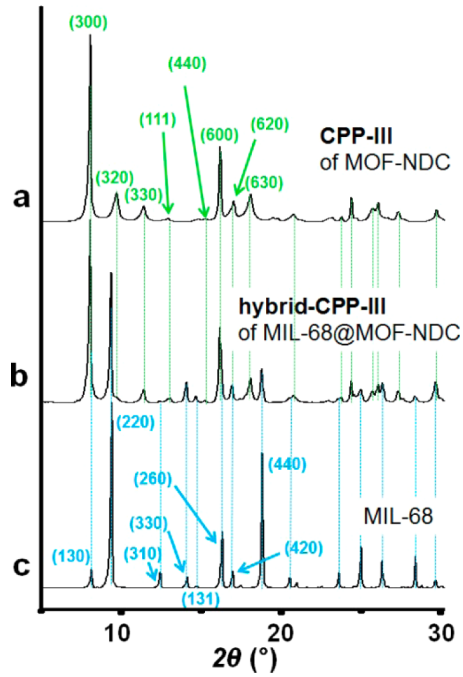

Figure 4. PXRD patterns of (a) **CPP-III** of MOF-NDC, (b) **hybrid-CPP-III** of MIL-68@MOF-NDC, and (c) **CPP-I** of MIL-68.

NDC structures within the particles. All peaks from both the MIL-68 core and MOF-NDC shell were found in the PXRD pattern of **hybrid-CPP-III**. The ratio of BDC and NDC within the particles and thus the relative amounts of the MIL-68 core and MOF-NDC shell were determined to be 1:1.11 by integrating the peaks correlated to H_2BDC and H_2NDC in the ^{1}H NMR spectrum of **hybrid-CPP-III** (Figure 3e). The 1:1.11 molar ratio of the MIL-68 core and MOF-NDC shell within **hybrid-CPP-III** corresponds to the 1:1.30 weight ratio of the MIL-68 core and MOF-NDC shell. (For this calculation, we have assumed that MOF-NDC has a chemical formula of $[In(OH)(NDC)]_n$, similar to $[In(OH)(BDC)]_n$ for MIL-68.) The increasing amount of MOF-NDC on the MIL-68 template was relatively lower than that of MIL-68-Br, as verified from their final sizes (Figures 2c and 3c) and the relative ratios of the initial and secondary MOFs within **hybrid-CPP-II** (1:3.65) and **hybrid-CPP-III** (1:1.11). N_2 sorption isotherms of **hybrid-CPP-III** (MIL-68@MOF-NDC) revealed that its BET surface

DOI: 10.1021/jacs.6b08821
J. Am. Chem. Soc. 2016, 138, 14434–14440

area (1021 $m^2 g^{-1}$) and total pore volume (0.46 $cm^3 g^{-1}$) values are located between those of MIL-68 and MOF-NDC (Figure 3f). These values were quite similar to those (1017 $m^2 g^{-1}$ and 0.45 $cm^3 g^{-1}$, respectively) calculated from the simple sum of the 1:1.30 weight contributions of pure MIL-68 and MOF-NDC within **hybrid-CPP-III**.

This unusual anisotropic growth for the production of the unique semitubular particles can be understood on the basis of the cell parameter differences between MIL-68 and MOF-NDC. First, we must pay attention to the fact that the growth of MOF-NDC was very efficient on the six rectangular facets, which expose the *ac* plane of MIL-68. To grow efficiently on the *ac* plane of the MIL-68 structure, MOF-NDC should have an identical one-dimensional metal ion chain in the direction of the *c* axis and thus have an identical *c* cell parameter with the MIL-68 template. In addition, MOF-NDC should have an identical repeating unit in the direction of the *a* axis with the MIL-68 structure (Figure 5). Initially, a three-dimensional rhombic structure (Figure 5c) was considered to be a possible candidate for the MOF-NDC structure. When the one-dimensional metal ion chain is propagated in a zigzag, as described in Figure 5b, a three-dimensional hexagonal structure of MIL-68 (orthorhombic crystal system) should occur. On the other hand, when this one-dimensional metal ion chain is propagated in one direction, as described in Figure 5c, a three-dimensional rhombic structure (hexagonal crystal system) should be produced. However, no correlation between this imaginary rhombic structure and the obtained PXRD pattern of MOF-NDC was found. We then focused on its morphological features. In many cases, the morphology of MOFs and CPPs indicates their inner-structure information.[36−40] The square or rectangular facets of **CPP-III** made from MOF-NDC, instead of hexagonal facets, indicate that MOF-NDC possibly has a square or rectangular structure instead of a hexagonal or rhombic structure. A three-dimensional square structure (Figure 5d, tetragonal crystal system) was next considered as a possible structure of MOF-NDC. This three-dimensional square structure could possibly be formed from the simple adjustment of the angle between the organic building block wings (green lines in the schematic representation) interacting with the one-dimensional metal ion chain (Figure 5d).

This speculated three-dimensional square structure (Figure 5d) has well-matched lattices with the MIL-68 template in the direction of the *a* and *c* axes but has a mismatched lattice in the direction of the *b* axis; therefore, it can grow on the six rectangular facets (*ac* plane) but cannot grow on the two hexagonal facets (*ab* plane) of the MIL-68 template (Figure 5e). Finally, an analysis of PXRD patterns of MOF-NDC and MIL-68@MOF-NDC verified that MOF-NDC has a three-dimensional square structure. The measured PXRD pattern of MOF-NDC was well matched with the calculated pattern of the speculated three-dimensional square structure, as verified by the whole pattern fitting using MDI Jade 9.0 software (Figure S8). The unit cell parameters of MOF-NDC calculated using MDI Jade 9.0 software were $a = b = 32.765$ Å, $c = 7.182$ Å, and $\alpha = \beta = \gamma = 90°$ (Figure S8); these values, specifically the *a* and *c* cell parameters, were well matched with those of MIL-68. The repeating distance between two metal ion chains (two blue dots in Figure 5b) of the three-dimensional hexagonal structure of MIL-68 is 10.887 Å, and that (two blue dots in Figure 5d) of the three-dimensional square structure of MOF-NDC is calculated to be 10.922 Å from its PXRD pattern. Finally, six intensive PXRD peaks (Figure 4a) of MOF-NDC at $2\theta = 8.10$,

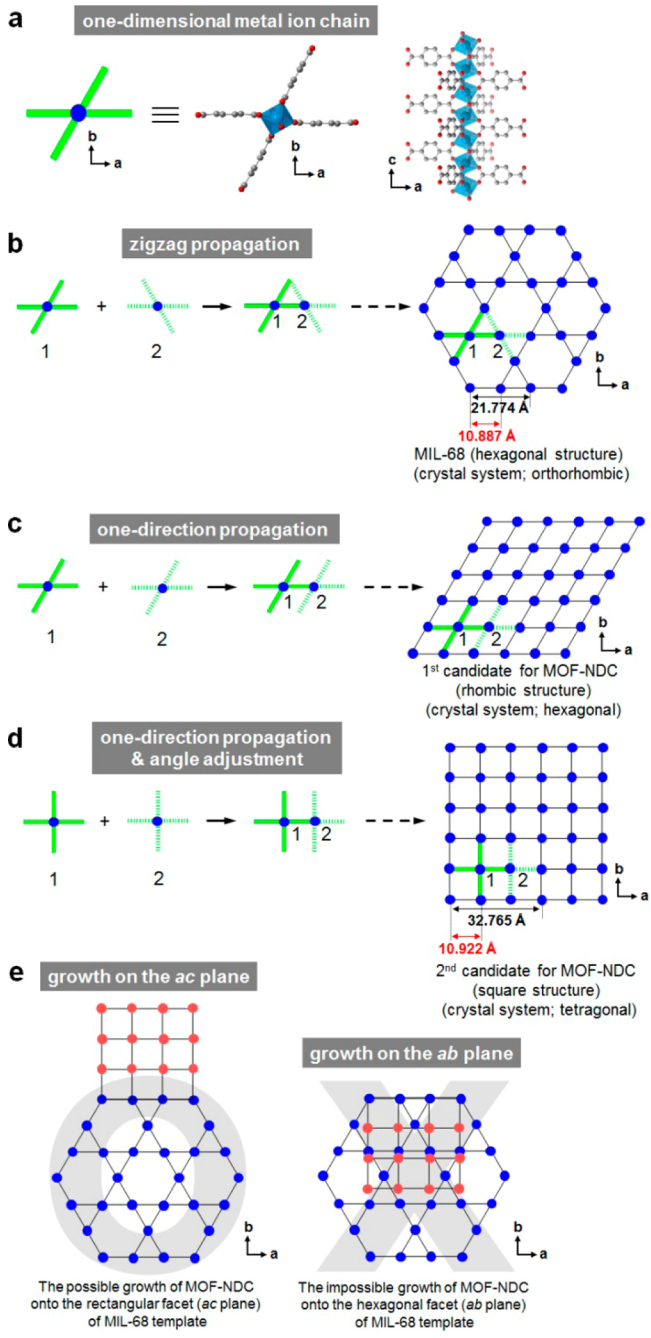

Figure 5. (a) Schematic and ball-and-stick representations of a one-dimensional metal ion chain within the MOF (MIL-68 and MOF-NDC). (b) Zigzag propagation of one-dimensional metal ion chains (metal ion chains 1 and 2) for the formation of a three-dimensional hexagonal structure of MIL-68 (orthorhombic crystal system). (c) One-direction propagation of one-dimensional chains for the formation of a three-dimensional rhombic structure (hexagonal crystal system). (d) One-direction propagation of one-dimensional chains for the formation of a three-dimensional square structure of MOF-NDC (tetragonal crystal system). (e) Possible growth of MOF-NDC on the rectangular facets (*ac* plane) of the MIL-68 template (left). The impossible growth of MOF-NDC on the hexagonal facets (*ab* plane) of the MIL-68 template (right). The distance between two metal ion chains (two blue dots in Figure 5b) of MIL-68 is 10.887 Å, and that (two blue dots in panel d) of MOF-NDC is calculated to be 10.922 Å from its PXRD pattern.

DOI: 10.1021/jacs.6b08821
J. Am. Chem. Soc. 2016, 138, 14434−14440

9.74, 11.44, 16.22, 17.06, and 18.12° were assigned to the (300), (320), (330), (600), (620), and (630) planes of the three-dimensional square structure, respectively.

Additional evidence for the rationale of the anisotropic growth of MOF-NDC on the *ac* plane (six rectangular facets) of the MIL-68 template was obtained from the SAED data (Figures 6 and 7). The simulated SAED patterns of the MIL-68

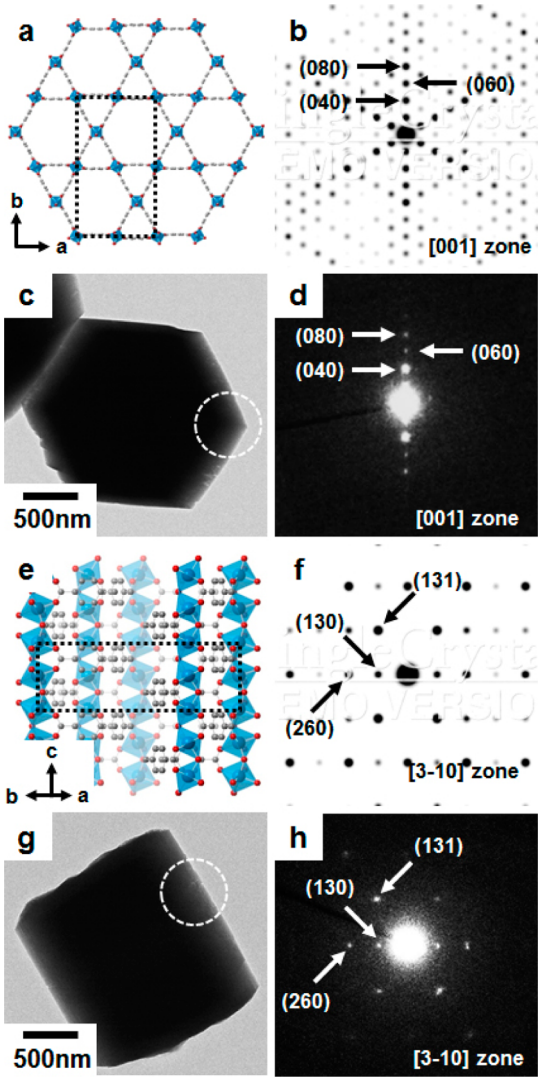

Figure 6. (a) Crystal structure of MIL-68 projected along the [001] zone axis. (b) Simulated SAED pattern of MIL-68 along the [001] zone axis. (c) TEM image of the MIL-68 template and (d) experimental SAED pattern of MIL-68 obtained from the region marked with a circle in c. (e) Crystal structure of MIL-68 projected along the [3−10] zone axis. (f) Simulated SAED pattern of MIL-68 along the [3−10] zone axis. (g) TEM image of the MIL-68 template and (h) SAED pattern of MIL-68 obtained from the region marked with a circle in g.

structure along the [001] and [3−10] zone axes were obtained by using SingleCrystal version 2.3.3 software (Figure 6b,f). The experimental SAED patterns of the MIL-68 template (Figure 6d,h) were well matched with the simulated SAED patterns. Strong spots for Bragg reflections of (040), (060), (080), (130), (131), and (260) were observed in the experimental SAED patterns of MIL-68 template. The *d*-spacing values of $d_{(040)}$, $d_{(130)}$, and $d_{(131)}$ were 9.202, 10.538, and 5.631 Å,

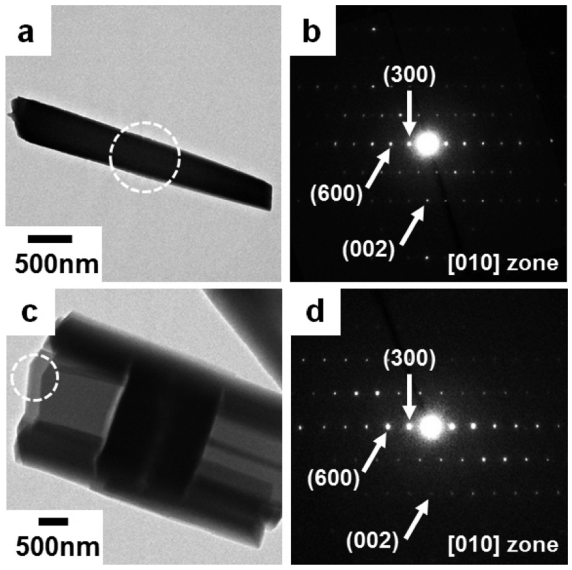

Figure 7. (a) TEM image of **CPP-III** and (b) SAED pattern of MOF-NDC obtained from the region marked with a circle in a. (c) TEM image of **hybrid-CPP-III** (MIL-68@MOF-NDC) and (d) SAED pattern of the MOF-NDC shell part obtained from the region marked with a circle in c.

respectively. The cell parameters of the MIL-68 template derived from these SAED patterns were a = 21.076, b = 36.808, and c = 6.823 Å. Note that there is a slight deviation in these derived cell parameters compared to those obtained from the single-crystal structure (a = 21.774, b = 37.677, and c = 7.233 Å) possibly because of the slight destruction during the SAED measurement. The SAED patterns of **CPP-III** and **hybrid-CPP-III** are displayed in Figure 7. The SAED pattern of the shell part of **hybrid-CPP-III** (Figure 7d) was exactly identical to the SAED pattern of MOF-NDC measured from **CPP-III** (Figure 7b), which indicated that the shell part of **hybrid-CPP-III** is identical to the MOF-NDC. The *d*-spacing values of $d_{(300)}$ and $d_{(002)}$ were 10.713 and 3.458 Å for **CPP-III** and 10.764 and 3.443 Å for **hybrid-CPP-III**, respectively. The cell parameters of MOF-NDC derived from the SAED pattern of **hybrid-CPP-III** were a = b = 32.292 Å and c = 6.886 Å. The a and c cell parameters of MOF-NDC are well matched with those of the MIL-68 template (3/2a = 31.614 Å and c = 6.823 Å), but the b cell parameter of MOF-NDC is not correlated with that of the MIL-68 template (b = 36.808 Å). These SAED studies again support the motive for the unusual anisotropic growth of MOF-NDC on the *ac* plane of the MIL-68 template.

■ CONCLUSIONS

We have demonstrated the fascinating isotropic and anisotropic growth of two MOFs, MIL-68 analog (MIL-68-Br) and nonanalog (MOF-NDC), on the MIL-68 template. The isotropic growth of MIL-68-Br over the entire surface of the MIL-68 template progressed to form core−shell-type MIL-68@MIL-68-Br. However, the unique anisotropic growth of MOF-NDC on the six rectangular facets (*ac* plane of the MIL-68 structure) but not on the two hexagonal facets (*ab* plane) of the MIL-68 template produced abnormal semitubular particles. In addition, the structural features of MOF-NDC were successfully speculated for the first time by considering its unique growth behavior and morphological characteristics; the validation of this structural speculation was confirmed from

DOI: 10.1021/jacs.6b08821
J. Am. Chem. Soc. 2016, 138, 14434−14440

the PXRD and SAED studies of MOF-NDC. The growth behavior and morphological features of MOFs should be considered to be important factors in the future for understanding the MOFs' structures. The construction of a well-defined MOF-on-MOF structure is essential for producing multifunctional MOFs and fine-tuning the properties of MOFs. The growth of MOF on MOF demonstrated here should provide noteworthy guidance for the rational construction of heterocompositional and functional MOF materials.

■ ASSOCIATED CONTENT

Supporting Information

The Supporting Information is available free of charge on the ACS Publications website at DOI: 10.1021/jacs.6b08821.

Experimental details and supporting figures and tables (PDF)

■ AUTHOR INFORMATION

Corresponding Author

*moh@yonsei.ac.kr

Author Contributions

S.C. and T.K. contributed equally.

Notes

The authors declare no competing financial interest.

■ ACKNOWLEDGMENTS

This work was supported by National Research Foundation of Korea (NRF) grants funded by the Korean government (MSIP) (nos. NRF-2012R1A2A1A03670409 and NRF-2015R1A2A1A15053777).

■ REFERENCES

(1) Furukawa, H.; Ko, N.; Go, Y. B.; Aratani, N.; Choi, S. B.; Choi, E.; Yazaydin, A. Ö.; Snurr, R. Q.; O'Keeffe, M.; Kim, J.; Yaghi, O. M. *Science* **2010**, *329*, 424−428.

(2) Farha, O. K.; Yazaydin, A. Ö.; Eryazici, I.; Malliakas, C. D.; Hauser, B. G.; Kanatzidis, M. G.; Nguyen, S. T.; Snurr, R. Q.; Hupp, J. T. *Nat. Chem.* **2010**, *2*, 944−948.

(3) Bohnsack, A. M.; Ibarra, I. A.; Bakhmutov, V. I.; Lynch, V. M.; Humphrey, S. M. *J. Am. Chem. Soc.* **2013**, *135*, 16038−16041.

(4) An, J.; Rosi, N. L. *J. Am. Chem. Soc.* **2010**, *132*, 5578−5579.

(5) Maji, T. K.; Matsuda, R.; Kitagawa, S. *Nat. Mater.* **2007**, *6*, 142−148.

(6) Herm, Z. R.; Wiers, B. M.; Mason, J. A.; van Baten, J. M.; Hudson, M. R.; Zajdel, P.; Brown, C. M.; Masciocchi, N.; Krishna, R.; Long, J. R. *Science* **2013**, *340*, 960−964.

(7) Tanabe, K. K.; Cohen, S. M. *Angew. Chem., Int. Ed.* **2009**, *48*, 7424−7427.

(8) Kozachuk, O.; Luz, I.; Llabrés i Xamena, F. X.; Noei, H.; Kauer, M.; Albada, H. B.; Bloch, E. D.; Marler, B.; Wang, Y.; Muhler, M.; Fischer, R. A. *Angew. Chem., Int. Ed.* **2014**, *53*, 7058−7062.

(9) Kreno, L. E.; Leong, K.; Farha, O. K.; Allendorf, M.; Van Duyne, R. P.; Hupp, J. T. *Chem. Rev.* **2012**, *112*, 1105−1125.

(10) Xu, H.; Chen, R.; Sun, Q.; Lai, W.; Su, Q.; Huang, W.; Liu, X. *Chem. Soc. Rev.* **2014**, *43*, 3259−3302.

(11) Sadakiyo, M.; Yamada, T.; Kitagawa, H. *J. Am. Chem. Soc.* **2011**, *133*, 11050−11053.

(12) Chen, B.; Wang, L.; Xiao, Y.; Fronczek, F. R.; Xue, M.; Cui, Y.; Qian, G. *Angew. Chem., Int. Ed.* **2009**, *48*, 500−503.

(13) Oh, M.; Mirkin, C. A. *Nature* **2005**, *438*, 651−654.

(14) Lee, H. J.; We, J.; Kim, J. O.; Kim, D.; Cha, W.; Lee, E.; Sohn, J.; Oh, M. *Angew. Chem., Int. Ed.* **2015**, *54*, 10564−10568.

(15) Pang, M.; Cairns, A. J.; Liu, Y.; Belmabkhout, Y.; Zeng, H. C.; Eddaoudi, M. *J. Am. Chem. Soc.* **2012**, *134*, 13176−13179.

(16) Zhang, Z.; Chen, Y.; Xu, X.; Zhang, J.; Xiang, G.; He, W.; Wang, X. *Angew. Chem., Int. Ed.* **2014**, *53*, 429−433.

(17) Tanaka, D.; Henke, A.; Albrecht, K.; Moeller, M.; Nakagawa, K.; Kitagawa, S.; Groll, J. *Nat. Chem.* **2010**, *2*, 410−416.

(18) Foucault-Collet, A.; Gogick, K. A.; White, K. A.; Villette, S.; Pallier, A.; Collet, G.; Kieda, C.; Li, T.; Geib, S. J.; Rosi, N. L.; Petoud, S. *Proc. Natl. Acad. Sci. U. S. A.* **2013**, *110*, 17199−17204.

(19) Della Rocca, J.; Liu, D.; Lin, W. *Acc. Chem. Res.* **2011**, *44*, 957−968.

(20) McKinlay, A. C.; Morris, R. E.; Horcajada, P.; Férey, G.; Gref, R.; Couvreur, P.; Serre, C. *Angew. Chem., Int. Ed.* **2010**, *49*, 6260−6266.

(21) Zhuang, J.; Kuo, C.-H.; Chou, L.-Y.; Liu, D.-Y.; Weerapana, E.; Tsung, C.-K. *ACS Nano* **2014**, *8*, 2812−2819.

(22) Horcajada, P.; Chalati, T.; Serre, C.; Gillet, B.; Sebrie, C.; Baati, T.; Eubank, J. F.; Heurtaux, D.; Clayette, P.; Kreuz, C.; Chang, J.-S.; Hwang, Y. K.; Marsaud, V.; Bories, P.-N.; Cynober, L.; Gil, S.; Férey, G.; Couvreur, P.; Gref, R. *Nat. Mater.* **2010**, *9*, 172−178.

(23) Lu, G.; Li, S.; Guo, Z.; Farha, O. K.; Hauser, B. G.; Qi, X.; Wang, Y.; Wang, X.; Han, S.; Liu, X.; DuChene, J. S.; Zhang, H.; Zhang, Q.; Chen, X.; Ma, J.; Loo, S. C. J.; Wei, W. D.; Yang, Y.; Hupp, J. T.; Huo, F. *Nat. Chem.* **2012**, *4*, 310−316.

(24) Zhao, M.; Deng, K.; He, L.; Liu, Y.; Li, G.; Zhao, H.; Tang, Z. *J. Am. Chem. Soc.* **2014**, *136*, 1738−1741.

(25) Aijaz, A.; Akita, T.; Tsumori, N.; Xu, Q. *J. Am. Chem. Soc.* **2013**, *135*, 16356−16359.

(26) Jo, C.; Lee, H. J.; Oh, M. *Adv. Mater.* **2011**, *23*, 1716−1719.

(27) Lee, H. J.; Cho, W.; Oh, M. *Chem. Commun.* **2012**, *48*, 221−223.

(28) Esken, D.; Turner, S.; Wiktor, C.; Kalidindi, S. B.; Van Tendeloo, G.; Fischer, R. A. *J. Am. Chem. Soc.* **2011**, *133*, 16370−16373.

(29) Fukushima, T.; Horike, S.; Kobayashi, H.; Tsujimoto, M.; Isoda, S.; Foo, M. L.; Kubota, Y.; Takata, M.; Kitagawa, S. *J. Am. Chem. Soc.* **2012**, *134*, 13341−13347.

(30) Hirai, K.; Furukawa, S.; Kondo, M.; Uehara, H.; Sakata, O.; Kitagawa, S. *Angew. Chem., Int. Ed.* **2011**, *50*, 8057−8061.

(31) Zhuang, J.; Chou, L.-Y.; Sneed, B. T.; Cao, Y.; Hu, P.; Feng, L.; Tsung, C.-K. *Small* **2015**, *11*, 5551−5555.

(32) Li, T.; Sullivan, J. E.; Rosi, N. L. *J. Am. Chem. Soc.* **2013**, *135*, 9984−9987.

(33) Lee, H. J.; Cho, Y. J.; Cho, W.; Oh, M. *ACS Nano* **2013**, *7*, 491−499.

(34) Furukawa, S.; Hirai, K.; Nakagawa, K.; Takashima, Y.; Matsuda, R.; Tsuruoka, T.; Kondo, M.; Haruki, R.; Tanaka, D.; Sakamoto, H.; Shimomura, S.; Sakata, O.; Kitagawa, S. *Angew. Chem., Int. Ed.* **2009**, *48*, 1766−1770.

(35) Volkringer, C.; Meddouri, M.; Loiseau, T.; Guillou, N.; Marrot, J.; Férey, G.; Haouas, M.; Taulelle, F.; Audebrand, N.; Latroche, M. *Inorg. Chem.* **2008**, *47*, 11892−11901.

(36) Cho, W.; Lee, H. J.; Oh, M. *J. Am. Chem. Soc.* **2008**, *130*, 16943−16946.

(37) Choi, S.; Lee, H. J.; Kim, T.; Oh, M. *Eur. J. Inorg. Chem.* **2014**, *2014*, 6220−6224.

(38) Ni, Z.; Masel, R. I. *J. Am. Chem. Soc.* **2006**, *128*, 12394−12395.

(39) Cho, W.; Park, S.; Oh, M. *Chem. Commun.* **2011**, *47*, 4138−4140.

(40) McGuire, C. V.; Forgan, R. S. *Chem. Commun.* **2015**, *51*, 5199−5217.

DOI: 10.1021/jacs.6b08821
J. Am. Chem. Soc. 2016, 138, 14434−14440